Activation of Diazene and the Nitrogenase Problem: An Investigation of Diazene-Bridged Fe(II) Centers with Sulfur Ligand Sphere. 1. Electronic Structure

Nicolai Lehnert,[†] Beatrix E. Wiesler,[†] Felix Tuczek,*[,†] Andreas Hennige,[‡] and Dieter Sellmann[‡]

Contribution from the Institut für Anorganische Chemie und Analytische Chemie der Universität Mainz, Staudinger Weg 9, D-55099 Mainz, Germany, and Institut für Anorganische Chemie der Universität Erlangen-Nürnberg, Egerlandstrasse 1, D-91058 Erlangen, Germany

Received February 7, 1997[⊗]

Abstract: Mössbauer and UV−vis spectroscopic measurements of the two diazene-bridged systems [{Fe'N_HS_4'}$_2$-(N_2H_2)] ('N_HS_4'$^{2-}$ = 2,2′-bis(2-mercaptophenylthio)diethylamine(2−)) and [{Fe'S_4'(PPr_3)}$_2$(N_2H_2)] ('S_4'$^{2-}$ = 1,2-bis(2-mercaptophenylthio)ethane(2−)) have been combined with self-consistent-field Xα scattered-wave (SCF-Xα -SW) calculations in order to describe the electronic properties of diazene coordinated to Fe(II)−sulfur centers. For both model systems, the experiments and calculations indicate a Fe(II)−N_2H_2−Fe(II) structure with Fe(II) low-spin centers. The stabilization of diazene is due to σ-donation from its highest occupied MO and π -backbonding into its lowest unoccupied MO (LUMO). The intense absorption band at approximately 600 nm is ascribed to a charge-transfer transition from metal-d orbitals into the diazene LUMO. Importantly, the diazene LUMO also is the LUMO of the complexes and is located between the fully occupied t_{2g}^* and empty e_g^* orbitals of the iron centers. It is concluded that the Fe(II) high-spin configuration present in a sulfur environment of lower ligand-field strength leads to reduction of diazene. Therefore diazene is likely to be involved in a reduction pathway of dinitrogen bound symmetrically (i.e., with both nitrogen atoms) to the iron−molybdenum cofactor (FeMoCo) of the enzyme nitrogenase.

Introduction

Nitrogen fixation is one of the fundamental synthetic processes of nature. It is catalyzed by the enzyme nitrogenase, the structure of which has been solved several years ago.[1] There is evidence that the bonding and reduction of dinitrogen proceeds at the iron−molybdenum cofactor (FeMoCo) in the MoFe protein of nitrogenase. However, neither the location and mode of dinitrogen bonding to the cofactor nor the reduction pathway to NH_3 are known.[2] The understanding of these processes at a molecular level remains one of the major tasks of chemistry.

Information relevant to the bonding, activation, and reduction of N_2 at the FeMoCo of nitrogenase can be obtained from the study of small-molecule model systems. Activation means that the N_2 moiety obtains some basicity through electron donation from the metal center(s). There exist numerous examples of dinitrogen complexes of transition metals. In the majority of these compounds, N_2 coordinates either terminally end-on to a single metal center or linear bridging between two centers.[3] In a few examples, N_2 also bridges in the side-on or edge-on (μ-η^2:η^2)) geometry.[4] Calculations indicate that the terminal end-on and the side-on/edge-on bridging modes may be candidates for N_2 bonding to the FeMoCo.[5] Furthermore, the reduction and protonation of dinitrogen bound to transition-metal centers have been studied intensively.[6] A well-known example is the reduction of N_2, bound terminally end-on in Mo(0)− and W(0)−N_2 complexes, to NH_3.[7] The asymmetric coordination of N_2 causes a negative partial charge at the β-nitrogen atom which in turn allows successive protonation of the N_2 moiety to diazenido, hydrazido, and hydrazidium complexes. Upon further protonation, the latter species dissociates into one molecule of NH_3 and the metal-imino complex, which again is protonated to give a second equivalent of ammonia. Importantly, both the protonation of the β-nitrogen, promoted by its negative partial charge, as well as the formation of a metal-N multiple bond contribute to the cleavage of the N−N triple bond.

* Corresponding author.
† Universität Mainz.
‡ Universität Erlangen-Nürnberg.
⊗ Abstract published in *Advance ACS Abstracts,* August 15, 1997.

(1) (a) Kim, J.; Rees, D. C. *Science* **1992**, *257*, 1677. (b) Kim, J.; Rees, D. C. *Nature* **1992**, *360*, 553. (c) Chan, M. K.; Kim, J., Rees, D. C. *Science* **1993**, *260*, 792. (d) Bolin, J. T.; Ronco, A. E., Morgan, T. V.; Mortenson, L. E.; Xuong, N. H. *Proc. Natl. Acad. Sci. U.S.A.* **1993**, *90*, 1078. (e) Chen, J.; Christiansen, J.; Campobasso, N.; Bolin, J. T.; Tittsworth, R. C.; Hales, B. J.; Rehr, J. J.; Cramer, S. P. *Angew. Chem.* **1993**, *105*, 1661.

(2) (a) Orme-Johnson, W. H. *Science* **1992**, *257*, 1639. (b) *Molybdenum Enzymes, Cofactors and Model Systems*; Stiefel, E. I., Coucouvanis, D., Newton, W. E., Eds.; American Chemical Society: Washington, D.C., 1993.

(3) (a) Hidai, M.; Mizobe, Y. *Chem. Rev.* **1995**, *95*, 1115. (b) Sutton, D.; *Chem. Rev.* **1993**, *93*, 995. (c) Chatt, J.; Dilworth, J. R.; Richards, R. L. *Chem. Rev.* **1978**, *78*, 589. (d) Henderson, R. A.; Leigh, G. J.; Pickett, C. J. *Adv. Inorg. Chem. Rad. Chem.* **1983**, *27*, 197.

(4) (a) Duchateau, R.; Gambarotta, S.; Beydoun, N.; Bensimon, C. *J. Am. Chem. Soc.* **1991**, *113*, 8986. (b) Fryzuk, M. D.; Haddad, T. S.; Mylvaganam, M.; McConville, D. H.; Rettig, S. J. *J. Am. Chem. Soc.* **1993**, *115*, 2782.

(5) (a) Plass, W. *J. Mol. Struc. (Theochem)* **1994**, *315*, 53. (b) Dance, I. G. *Aust. J. Chem.* **1994**, *47*, 979. (c) Deng, H.; Hoffmann, R. *Angew. Chem.* **1993**, *105*, 1125.

(6) (a) Leigh, G. J. *Acc. Chem. Res.* **1992**, *25*, 177. (b) Shilov, A. E. *Pure Appl. Chem.* **1992**, *64*, 1409.

(7) (a) Jimenez-Tenorio, M.; Puerta, M. C.; Valerga, P.; Hughes, D. L. *J. Chem. Soc. Dalton Trans.* **1994**, 2431. (b) George, T. A.; Kaul, B. B.; Chen, Q.; Zubieta, J. *Inorg. Chem.* **1993**, *32*, 1706. (c) Barclay, J. E.; Hills, A.; Hughes, D. L.; Leigh, G. J.; Macdonald, C. J.; Abu Bakar, M.; Mohd.-Ali, H. *J. Chem. Soc., Dalton Trans.* **1990**, 2503. (d) George, T. A.; Ma, L.; Shailh, S. N.; Tisdale, R. C.; Zubieta, J. *Inorg. Chem.* **1990**, *29*, 4789. (e) Galindo, A.; Hills, A.; Hughes, D. L.; Richards, R. L.; Hughes, M; Mason, J. *J. Chem. Soc., Dalton Trans.* **1990**, 283. (f) Abu Bakar, M.; Hughes, D. L.; Hussain, W.; Leigh, G. J.; Macdonald, C. J.; Mohd.-Ali, H. *J. Chem. Soc., Dalton Trans.* **1988**, 2545. (g) Henderson, R. A. *J. Chem. Soc., Dalton Trans.* **1984**, 2259. (h) Henderson, R. A. *J. Chem. Soc., Dalton Trans.* **1982**, 917. (i) Hussain, W.; Leigh, G. J.; Pickett, C. J. *J. Chem. Soc., Chem. Commun.* **1982**, 747. (j) Takahashi, T.; Mizobe, Y.; Sato, M.; Uchida, Y.; Hidai, M.; *J. Am. Chem. Soc.* **1980**, *102*, 7461. (k) Chatt, J.; Pearman, A. J.; Richards, R. L. *J. Chem. Soc., Dalton Trans.* **1978**, 1767. (l) For references earlier than 1978 see ref 3c.

S0002-7863(97)00419-8 CCC: $14.00

According to Thorneley and Lowe,[8] this reduction pathway, starting from terminally end-on coordinated N_2, is also valid for nitrogenase.

The reduction of dinitrogen bound symmetrically, either side-on/edge-on[9] or linear end-on bridging in binuclear complexes, is less well defined.[6] In general, protonation of these systems, if possible, directly leads to hydrazine and/or ammonia, and no intermediates can be detected. An exception is the protonation of binuclear Nb(III)− and Ta(III)−N_2 complexes with dithiocarbamato coligands, where spectroscopic evidence for N_2H- and N_2H_3-bridged intermediates could be obtained.[10] At the μ-$NHNH_2$ stage the binuclear complex breaks apart, and further reduction to N_2H_4 proceeds at a single metal center. In this case, however, the bridging N_2 ligand is already activated to the hydrazido(4−) level in the starting compounds, and the subsequent chemical transformations correspond to successive protonations of this moiety. In the kinetic scheme of nitrogenase by Thorneley and Lowe,[8] on the other hand, protonation and reduction of N_2 occur stepwise and concomitantly.

In order to obtain insight into a reduction pathway relevant to nitrogenase but involving symmetrically-bound N_2, the isolation and characterization of individual members of the series

$$\mathrm{M{-}N_2{-}M} \xrightarrow[2H^+]{2e^-} \mathrm{M{-}N_2H_2{-}M} \xrightarrow[2H^+]{2e^-} \mathrm{M{-}N_2H_4{-}M} \xrightarrow[2H^+]{2e^-} 2\ \mathrm{M{-}NH_3} \quad (1)$$

is of considerable interest. Collman et al. have achieved this for all species appearing in eq 1 with a ruthenium cofacial diporphyrin.[11] However, interconversions between the individual intermediates are only possible via successive two-electron oxidation reactions, i.e., in a direction opposite to eq 1. Based on these results, the authors have analyzed in a detailed way the requirements to be met in order to achieve the electrocatalytic reduction of dinitrogen according to eq 1. They have pointed out that, while the reduction from N_2 to N_2H_2 (diazene) can be assumed to be the most difficult step, also subsequent steps (such as the reduction of N_2H_4 to 2 NH_3) may encounter serious thermodynamic barriers. Thus, complexes allowing the electrocatalytic reduction of N_2 must fulfill numerous conditions in a subtle way, and the same holds for the further reduction of the intermediates such as diazene.

Diazene is highly unstable in its free state but can be stabilized by coordination to metal complex fragments.[12−14] Iron−sulfur diazene complexes have been prepared by air-oxidation of the corresponding mono- or binuclear hydrazine complexes.[13,14] The preparation has also been realized directly from diazene generated in situ by decomposition of potassium azodicarboxylate.[15] In these iron−diazene complexes, the diazene ligand appears to be highly stable toward reduction. Whereas the cyclic voltammogram exhibits a number of redox waves in the range between −0.1 and +1.0 V, no redox wave has been observed in the cathodic range, indicating that reduction of the diazene to the hydrazine complex cannot be achieved at accessible potentials. Since the diazene unit cannot be protonated directly, questions arise as to why diazene is so highly stabilized or *vice versa* so little activated toward transformation to hydrazine and how activation toward this reaction could be achieved.

Table 1. Parameters of the Mössbauer Spectra

compd	T (K)	isomer shift δ^a (mm/s)	quadrupole splitting ΔQ (mm/s)
"N_HS_4" (I)	298	0.2917	1.1092
	10	0.3900	1.1742
"S_4P" (II)	298	0.2570	0.8230
	10	0.3491	0.8795

[a] Relative to α-iron.

This study concerns two trans-μ-1,2 Fe(II)−diazene complexes, [{Fe'N_HS_4'}$_2$(N_2H_2)] (I)[13] and [{Fe'S_4'(PPr_3)}$_2$(N_2H_2)] (II),[14] both of which are structurally characterized. The iron centers are coordinated octahedrally by four sulfur ligands (two thiolate, two thioether groups) and one amine (I) or phosphine (II) ligand trans (I) or cis (II) to the bridging diazene unit, respectively. The overall point group symmetry of I and II is C_i, while the planar $Fe_2(N_2H_2)$ unit has C_{2h} symmetry. Due to the sulfur environment of the iron centers, these systems are, to date, the closest models for the binding of a N_2 species to the FeMoCo.[16] The stabilization of diazene, which is highly reactive as a free molecule, has been mainly attributed to formation of a four-center-6π -electron system, steric shielding by the 'N_HS_4' ligand, and the existence of strong tricentric S···H−N hydrogen bonds, the contribution of which to the heat of formation of the complexes has been estimated to be 80 kJ/mol.[13] Both complexes are diamagnetic. The visible absorption spectra of I and II show an intense band at 580 and 620 nm, respectively, which is absent in [{Fe'S_4'(PPr_3)$_2$}], an analogue of II with similar ligand geometry around the iron. This absorption band has been assigned to an electronic transition within the four-center-6π -electron system. In order to obtain quantitative insight into the electronic factors determining the stabilization of diazene by Fe−S centers and the properties of this structure with respect to further reduction, we have carried out Mössbauer spectroscopic and optical absorption studies on I and II as well as self-consistent-field Xα scattered-wave (SCF-Xα-SW) calculations on idealized structures of I and II. These investigations are complemented by Raman and IR spectroscopic studies which are presented in part 2 of this paper. The consequences of the resulting electronic structure description with respect to a possible role of diazene in the reduction of dinitrogen by nitrogenase are considered.

Experimental and Computational Procedures

Sample Preparation. Complex I and II with natural abundance isotopes were prepared as described before by (a) air oxidation of hydrazine precursors[13,14] or (b) directly by the azodicarboxylate method.[15]

Mössbauer and UV−vis Spectroscopy. Variable-temperature Mössbauer spectra of complex I and II were obtained on a standard Mössbauer setup equipped with an Oxford helium flow cryostat. Samples were kept in a plexiglass holder; the source was ^{57}Co/Rh. Data acquisition was performed with the VKS system (Darmstadt University).

(8) Thornley, R. N. F.; Lowe, D. J. In *Molybdenum Enzymes*; Spiro, T. G., Ed.; John Wiley: 1985.
(9) Schrock, R. R.; Glassman, T. E.; Vale, M. G.; Kol, M. *J. Am. Chem. Soc.* **1993**, *115*, 1760.
(10) Dilworth, J. R.; Henderson, R. A.; Hills, A.; Hughes, D. L.; Macdonald, C.; Stephens, A. N.; Walton, D. R. M. *J. Chem. Soc., Dalton Trans.* **1990**, 1077.
(11) (a) Collman, J. P.; Hutchison, J. E.; Lopez, M. A.; Guilard, R.; Reed, R. A. *J. Am. Chem. Soc.* **1991**, *113*, 2794. (b) Collman, J. P.; Hutchison, J. E.; Lopez, M. A.; Guilard, R. *J. Am. Chem. Soc.* **1992**, *114*, 8066. (c) Collman, J. P.; Hutchison, J. E.; Ennis, M. S.; Lopez, M. A.; Guilard, R. *J. Am. Chem. Soc.* **1992**, *114*, 8074.
(12) (a) Sellmann, D. *J. Organomet. Chem.* **1972**, *44*, C46. (b) Sellmann, D.; Brandl, A.; Endell, R. *J. Organomet. Chem.* **1975**, *90*, 309. (c) Smith, M. R., III; Cheng, T.-Y.; Hillhouse, G. L. *J. Am. Chem. Soc.* **1993**, *115*, 8638. (d) Cheng, T.-Y.; Ponce, A.; Rheingold, A. L.; Hillhouse, G. L. *Angew. Chem.* **1994**, *106*, 703.
(13) Sellmann, D.; Soglowek, W.; Knoch, F.; Moll, M. *Angew. Chem.* **1989**, *101*, 1244.
(14) Sellmann, D.; Friedrich, H.; Knoch, F.; Moll, M. *Z. Naturforsch.* **1994**, *48b*, 76.
(15) Sellmann, D.; Hennige, A. *Angew. Chem.* **1997**, *109*, 270.
(16) Richards, R. L. *Pure App. Chem.* **1996**, *68*, 1521.

Table 2. Coordinates and Parameters of the Asymmetric Units of $\tilde{I}$ and $\tilde{II}$[a]

no.	atom	position (x, y, z)[b]			radius[b]	α
			$[\{Fe(NH_3)(SH)_2(SH_2)_2\}_2(N_2H_2)]$ ($\tilde{I}$)			
1	out	0.0000	0.0000	0.0000	10.4028	0.73804
2	N2	−0.7252	0.9913	0.0000	1.6579	0.75197
3	H2	−2.7388	0.1271	0.0000	1.3040	0.77725
4	Fe1	0.0000	4.4487	0.0000	2.2801	0.71151
5	S1	4.2568	3.5589	0.0000	2.4770	0.72475
6	S2	0.0000	4.4487	−4.3464	2.3472	0.72475
7	S3	−4.2567	5.3385	0.0000	2.4850	0.72475
8	N1	0.7897	8.2342	0.0000	1.6931	0.75197
9	H1	5.3911	5.8171	0.0000	1.3649	0.77725
10	H2/1	−2.5088	4.8377	−4.3464	1.3575	0.77725
11	H2/2	0.3890	6.9576	−4.3464	1.3552	0.77725
12	H3	−4.6541	7.8341	0.0000	1.3645	0.77725
13	H1/1	−0.8193	9.2814	0.0000	1.1853	0.77725
14	H1/2	1.8011	8.7399	1.5685	1.1909	0.77725
			$[\{Fe(PH_3)(SH)_2(SH_2)_2\}_2(N_2H_2)]$ ($\tilde{II}$)			
1	out	0.0000	0.0000	0.0000	10.9394	0.73557
2	N2	0.0000	1.2094	0.0000	1.6348	0.75197
3	H2	1.9275	1.7197	0.0000	1.2161	0.77725
4	Fe1	−2.6645	3.6094	0.0000	2.2821	0.71151
5	S1	0.2646	6.8597	0.0000	2.4944	0.72475
6	S2	−5.8393	6.4629	0.0000	2.3293	0.72475
7	S3	−2.6645	3.6094	4.3275	2.3383	0.72475
8	S4	−5.5936	0.3590	0.0000	2.4772	0.72475
9	P1	−2.6645	3.6094	−4.2708	2.3378	0.72620
10	H1	−1.1149	8.9762	0.0000	1.3522	0.77725
11	H2/1	−4.1385	8.3526	0.0000	1.3451	0.77725
12	H2/2	−5.8393	6.4629	2.5322	1.3222	0.77725
13	H3/1	−4.4600	5.4046	4.3275	1.3255	0.77725
14	H3/2	−4.4600	1.8141	4.3275	1.3458	0.77725
15	H4	−6.0282	−0.1323	2.4377	1.3521	0.77725
16	H1/1	−4.3464	5.1212	−5.7070	1.4627	0.77725
17	H1/2	−3.1369	1.3984	−5.7070	1.4627	0.77725
18	H1/3	−0.5102	4.3086	−5.7070	1.4642	0.77725

[a] The missing coordinates are generated by the use of symmetry operations like inversion or reflection at the central plane. [b] Coordinates and radii of the atoms in bohr (1 bohr = 0.52918 Å).

Spectra were fitted using the program MOSFUN.[17] UV−vis spectra of methylene chloride solutions of I and II were obtained with a Bruins Omega-10 spectrometer.

DFT-Calculations. Spin-restricted SCF-Xα -SW calculations have been performed for the singlet ground state of simplified models $\tilde{I}$ and $\tilde{II}$ of complexes I and II. The 1982 QCPE release of the SCF-Xα -SW package has been employed. Both systems carry no charge, and therefore no Watson sphere has been used. Convergence was reached when the largest relative change in the potential between subsequent iterations was less than 1×10^{-5}. The α-values (Table 2) were taken from the table of Schwarz,[18] and those in the inner- and outer-sphere regions were weighted averages of the atomic α -values based on the number of valence electrons in the neutral free atoms. All calculations were performed with Norman sphere radii of the involved atoms.

Results and Analysis

A. Mössbauer Spectroscopy. Figure 1 shows the Mössbauer spectra of the complexes I and II at 10 K. The corresponding parameters are given in Table 1 for 10 K and room temperature. Both systems exhibit simple doublets with quadrupole splittings of 0.8−1.2 mm/s and isomer shifts of 0.29−0.39 mm/s (I) and 0.26−0.35 mm/s (II), respectively (δ vs α-iron). These parameters exclude a Fe(II) high-spin configuration found in [Fe(L)'N_HS_4'] and [Fe(L)'S_4'] systems with L = N_2H_4 and TMEDA which corresponds to isomer shifts from 0.8−0.9 mm/s and quadrupole splittings of around 3 mm/s.[19] Fe(III) low-spin systems, on the other hand, exhibit smalleror negative isomer shifts and Fe(III) high-spin systems have larger isomer shifts. Hence, we conclude that the electronic configuration present in the Fe−diazene systems has to be described as Fe(II) low-spin. The Mössbauer parameters therefore may be related to those of the [Fe(CO)'N_HS_4'] complex which is Fe(II) low-spin as well. Its quadrupole splitting is somewhat smaller than that of complex I (0.84 vs 1.11 mm/s at room temperature) which can be ascribed to the binuclear geometry of I and the fact that CO forms two equivalent π-bonds with iron. Therefore the charge distribution has a higher symmetry in the CO than in the diazene complex. The fact that the isomer shift of the CO complex (0.13 mm/s at room temperature) is also smaller than that of I (0.29 mm/s) indicates that the π-acceptor strength of CO must be higher than that of diazene since backbonding into ligand π-orbitals reduces d-electron density which acts to decrease δ.[20] The assignment of a Fe(II) low-spin configuration to complex I and II is in accordance with bond length considerations in [Fe(L)'N_HS_4'] systems. Thus, the complexes with L = CO and $^1/_2$ N_2H_2 exhibit average Fe−S(thioether), Fe−S(thiolate), and Fe−N(amine) distances of 224, 229, and 205 pm, respectively, which are elongated on average by 35 pm (Fe−S(thioether)), 10 pm (Fe−S(thiolate)), and 20 pm (Fe−N(amine)) in the corresponding high-spin Fe(II) systems with L = N_2H_4, NH_3, and CH_3-OH. Thus, as already pointed out,[19] the [Fe(L)'N_HS_4'] system shows a borderline behavior between Fe(II) high-spin and low-spin depending upon the nature of the coligand L: with purely

(17) Müller, E. W. *Mössb. Eff. Ref. Data J.* **1981**, *4*, 89.
(18) (a) Schwarz, K. *Theor. Chim. Acta* **1974**, *34*, 225. (b) Schwarz, K. *Phys. Rev. B* **1972**, *5*, 2466.
(19) Sellmann, D.; Soglowek, W.; Knoch, F.; Ritter, G.; Dengler, R. *Inorg. Chem.* **1992**, *31*, 3711.
(20) Gütlich, P.; Link, R.; Trautwein, A. *Mössbauer Spectroscopy and Transition Metal Chemistry*; Springer Verlag: 1978.

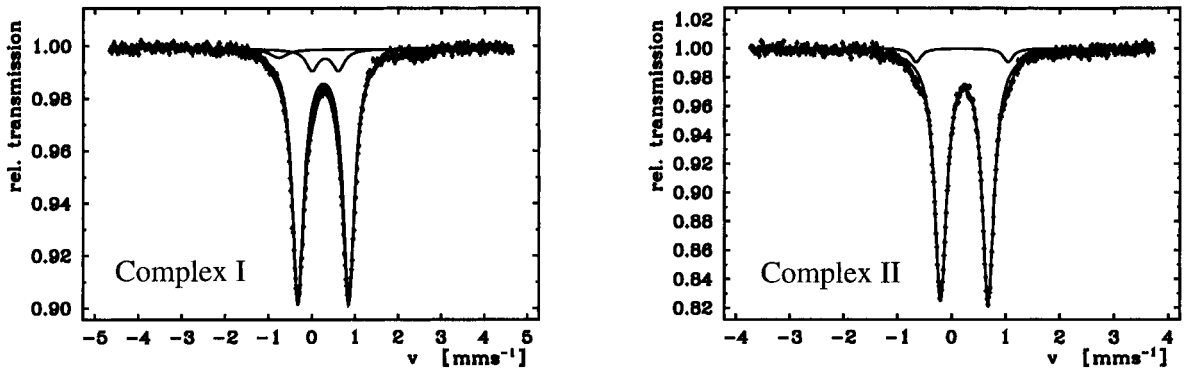

Figure 1. Mössbauer spectra of compounds I and II at 10 K along with fits.

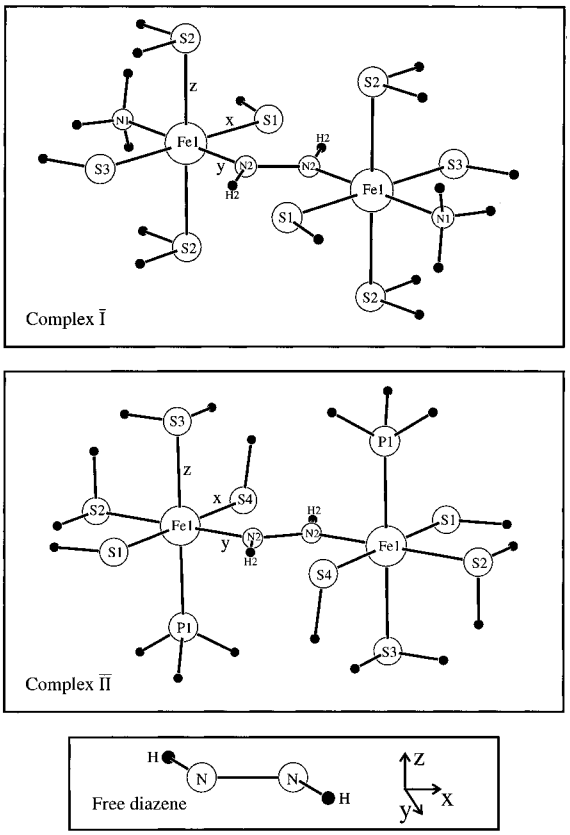

Figure 2. Structures of the model systems Ĩ and ĨĨ used for calculations and of free diazene along with coordinate systems. Note that the S−C (S−H) bonds of complex Ĩ have been rotated into the diazene plane. The orientations of the S−C (S−H) bonds of complex ĨĨ correspond to those of the X-ray structure.

σ-donating ligands, the Fe(II) configuration is high-spin, with σ-donating and π-accepting ligands, it is low-spin.

The weak doublets observed in the spectra of both compounds I and II (see Figure 1) belong to impurities.

B. DFT-Calculations. The structures of the models used for calculation [{Fe(NH$_3$)(SH)$_2$(SH$_2$)$_2$}$_2$(N$_2$H$_2$)] Ĩ and [{Fe(PH$_3$)(SH)$_2$(SH$_2$)$_2$}$_2$(N$_2$H$_2$)] ĨĨ are given in Figure 2. They are related to the known crystal structures of the complexes I[13] and II[14] but simplified by saturating the atoms of the first coordination sphere of the iron centers with hydrogen. Since the Fe(II) centers in compounds I and II have a nearly octrahedral coordination geometry, all valence angles at the iron atoms were set to 90° in the model systems. The bond lengths taken were according to X-ray structure data of I and II. Bond angles and lengths of the hydrogen atoms in the "new" ligands -SH, -SH$_2$, -NH$_3$, and -PH$_3$ are based on the known data of the free molecules. The orientation of these ligands has been adjusted in such a way that the highest possible symmetry of the corresponding model system is reached. The resulting model complexes, Ĩ and ĨĨ, have C_{2h}- and C_i-symmetry, whereas the real compounds both are C_i. In order to set up an orbital correlation diagram, the MO-scheme of free diazene (geometry taken from the calculations of Pople and Curtiss[21]) has been calculated as well. Table 2 contains the parameters employed for the Xα calculations.

Molecular Orbitals of Free Diazene. The MO-scheme of free diazene is given in the middle column of Figure 3. Figure 4 shows the corresponding contour plots of the frontier orbitals, π_v^* and π_h^*. The π_v and π_v^* orbitals (vertical) are perpendicular to the *xy*-plane of the diazene unit and correspond to "real" π-bonds, while the orbitals π_h and π_h^* (horizontal) lie within the *xy*-plane and derive from the p-functions of the nitrogen atoms which are directed to the hydrogen atoms; these orbitals have σ-bonding character with respect to hydrogen. The orbitals π_v^* and π_v are the bonding and antibonding combinations of the p_z -functions of the nitrogen atoms with π_v^* being the LUMO of the molecule. Above the π-bonding orbital π_v, the HOMO π_h^* is located which emerges from the antibonding combination of the p_y-functions of the nitrogen atoms. In molecular N_2, π_h^* and π_v^* would be degenerate and both unoccupied. However, because of the bonding overlap with the 1s-functions of the hydrogen atoms, π_h^* is lowered in energy and doubly occupied. The second hydrogen-bonding orbital is π_h which results from the bonding combination of the p_y-functions. Due to its low energy, it is of little importance for the electronic structure of diazene complexes. The same holds for p_σ, the σ-bonding combination of the two p_x-orbitals along the N−N-axis and the σ-orbitals which are of mainly s character.

In the following sections we first discuss the MO-scheme of model compound Ĩ (Figure 3, left) and then compare it with the results obtained on model compound ĨĨ (Figure 3, right).

Stabilization of Diazene in Complex Ĩ. The HOMO of diazene, π_h^*, is strongly lowered in energy by a σ-interaction with the Fe(II) centers forming π_h^*–Fe(σ) (see Figure 3, left). This strong σ-donation of diazene to the d-orbitals (of type e_g) of iron is the main contribution to the stabilization of diazene in the complex. π_h^*–Fe(σ) is of Fe−N-, and N−H-bonding character. In addition, this orbital shows a nonzero electron density between the hydrogen atoms of diazene and the thiolate donors S_1 (see Figure 5) lying at short distance to them, which corresponds to the formation of two N−H···S hydrogen bridges. Further contributions to these hydrogen bridges are found in π_h and some Fe−sulfur-type orbitals of the e_g- and t_{2g}-blocks. Because of its low energetic position, π_h mostly interacts with iron s- and p-functions in a σ-bonding manner.

(21) Pople, J. A.; Curtiss, L. A. *J. Chem. Phys.* **1991**, *95*, 4385.

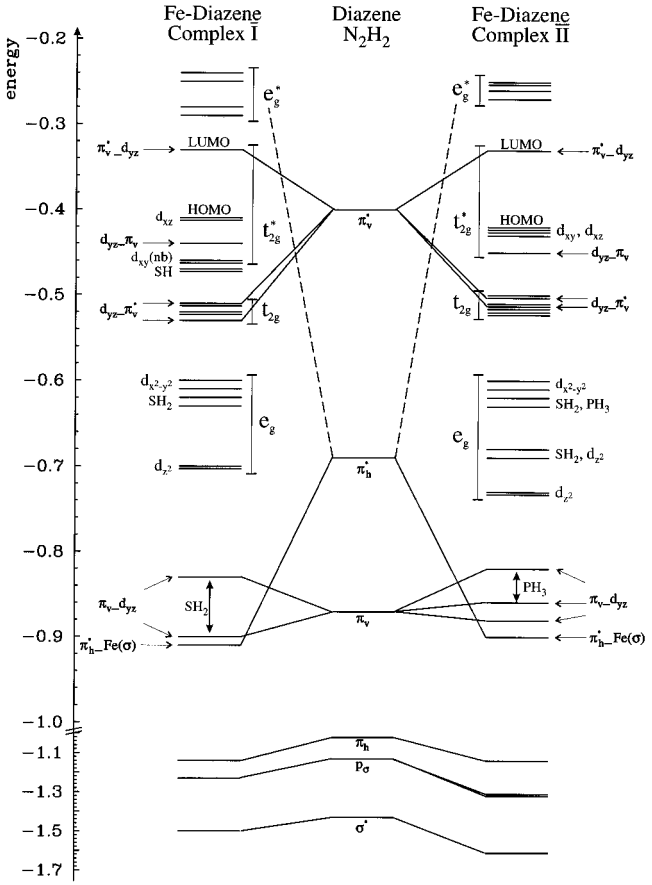

Figure 3. MO correlation diagram between free diazene and models Ĩ and ĨĨ indicating the principal bonding interactions (energy in Rydberg). MO designations correspond to those of Table 3 and Figure 5.

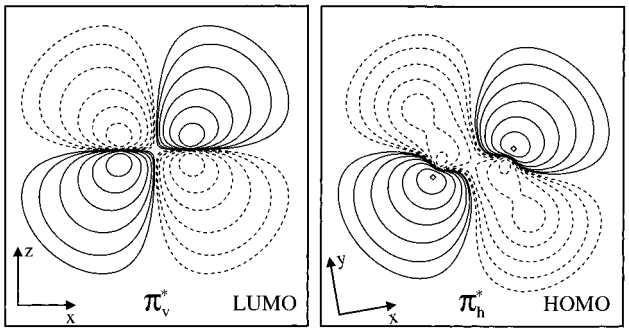

Figure 4. Contour plots of the frontier orbitals of diazene. Contours are located at ±0.32, 0.16, 0.08, 0.04, 0.02, and 0.01 [*e*/bohr^3]$^{1/2}$.

The diazene orbitals π_v and π_v^* overlap with the d_{yz} functions of iron as shown in Figure 5. The orbital π_v^* has an energetic position close to the frontier orbitals of iron and therefore shows strong mixing with the d_{yz} functions of the Fe(II) centers, more precisely with their combination of b_g-symmetry. Since π_v^* is higher in energy than d_{yz}, the LUMO of the iron−diazene complex, π_v^*_d_{yz}, mainly has diazene-π_v^* character (50% π_v^* charge contribution) with a smaller Fe(II)-d_{yz} participation (30%). The LUMO is both N−N- and Fe−N-antibonding. The bonding combination of π_v^* and the b_g-combination of d_{yz}, called d_{yz}–π_v^*, is found at much lower energy than the LUMO. This is caused by the strong π-interaction of the basis functions involved and represents the second-largest contribution to the iron−diazene bond. The d_{yz}–π_v^* orbital mixes with p-functions of the thiolate donors S_1 and S_3 and is therefore split into two orbitals having about 50% Fe-d and 10% π_v^* contribution (see Table 3a).

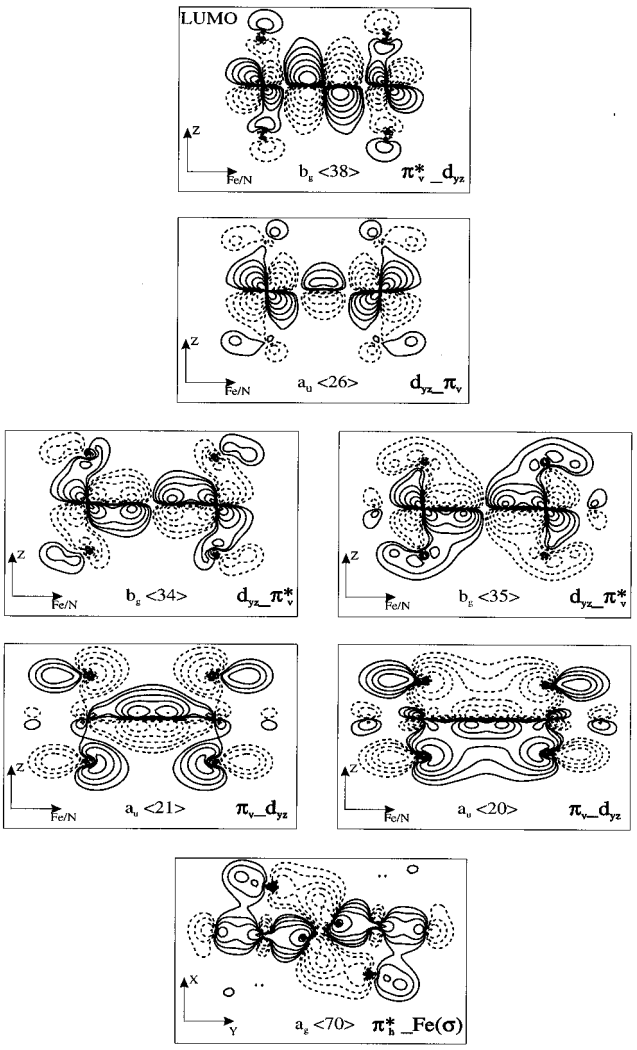

Figure 5. Contour plots of important molecular orbitals of Ĩ. Contours are located at ±0.32, 0.16, 0.08, 0.04, 0.02, and 0.01 [*e*/bohr^3]$^{1/2}$.

The orbital π_v is very low in energy and so the interaction with the Fe(II) centers is small. Therefore, the orbital d_{yz}–π_v has nearly pure metal character (charge contribution: 88% d_{yz}) with a small participation of π_v (3%). Correspondingly, the resulting diazene-type orbital π_v–d_{yz} almost has no iron contribution. The observed splittings are due to the interaction of π_v–d_{yz} with p-functions of the thioether donors S_2 lying above and below the Fe−N_2H_2−Fe-plane. Figure 5 shows the formed orbitals $a_u\langle 21\rangle$ and $a_u\langle 20\rangle$. The antibonding interaction between the thioether p-functions and π_v in $a_u\langle 21\rangle$, causing the rise in energy of this orbital as compared to the bonding combination in $a_u\langle 20\rangle$, is obvious. The orbital π_v–d_{yz} of complex ĨĨ even shows a triple splitting, since one of the thioether donors per Fe(II) center is substituted by a phosphine (see below).

Iron−Sulfur Interaction in Complex Ĩ. The Fe−S interaction determines the energy of most frontier orbitals and the orientation of the different d-orbitals of iron. Especially the p-functions of the thiolate donors strongly mix with the d-functions of iron causing an extended covalency between these atoms. To distinguish the different orbitals with Fe(II)-d contributions, the local labels "e_g" (σ-bonding and antibonding) and "t_{2g}" (π-bonding and antibonding) are used.

(i) Orbitals of Type e_g^* and e_g. The e_g^* symbol labels the σ-antibonding combinations of d_{z^2} and $d_{x^2-y^2}$ orbitals with p-functions of the thiolate ($S_1(p)/S_3(p) - d_{x^2-y^2}$) and thioether donors ($S_2(p) - d_{z^2}$). From these interactions four orbitals result, which all have about 50% Fe(II)-d contribution and 20%

Table 3. Charge Contributions of $\tilde{\mathrm{I}}$ and $\tilde{\mathrm{II}}$[a]

a. $[\{Fe(NH_3)(SH)_2(SH_2)_2\}_2(N_2H_2)]$ ($\tilde{\mathrm{I}}$)

orbital	label	energy (Rydberg)	charge decomposition[b] % N2	% H2	% Fe1	% S1	% S3	% S2	% N1
	$a_g\langle 78\rangle$	−0.2369	5	1	55	8	9	1	6
	$b_u\langle 57\rangle$	−0.2479	3	0	55	12	12	1	5
	$a_g\langle 77\rangle$	−0.2820	1	0	52	4	3	24	1
	$b_u\langle 56\rangle$	−0.2871	2	0	58	1	1	24	3
π^*_v–d_{yz}	$b_g\langle 38\rangle$	−0.3344	52	0	33	0	0	2	0
d_{xz}	$a_u\langle 25\rangle$	−0.4056	0	0	47	18	19	1	0
d_{xz}	$b_g\langle 37\rangle$	−0.4076	0	0	48	17	19	1	0
d_{yz}-π_v	$a_u\langle 26\rangle$	−0.4447	3	0	88	1	1	1	0
d_{xy} (nb)	$a_g\langle 76\rangle$	−0.4564	1	1	76	8	6	0	0
d_{xy} (nb)	$b_u\langle 55\rangle$	−0.4617	1	1	82	3	5	0	0
SH	$b_g\langle 36\rangle$	−0.4656	0	0	3	24	41	7	0
SH	$a_u\langle 24\rangle$	−0.4695	0	0	4	22	41	7	0
d_{yz}–π^*_v	$b_g\langle 34\rangle$	−0.5068	13	0	55	8	6	5	0
	$a_g\langle 74\rangle$	−0.5130	0	0	18	28	35	1	0
	$b_u\langle 54\rangle$	−0.5178	0	0	14	29	36	1	0
	$a_u\langle 23\rangle$	−0.5181	0	0	41	29	9	4	0
d_{yz}–π^*_v	$b_g\langle 35\rangle$	−0.5270	10	0	44	21	4	3	0
$d_{x^2-y^2}$	$b_u\langle 52\rangle$	−0.6053	0	0	31	31	22	0	1
$d_{x^2-y^2}$	$a_g\langle 75\rangle$	−0.6093	0	0	32	29	23	0	1
SH_2	$a_u\langle 22\rangle$	−0.6253	2	0	6	2	2	67	0
SH_2	$b_g\langle 33\rangle$	−0.6338	2	0	6	2	2	66	0
d_{z^2}	$b_u\langle 53\rangle$	−0.6961	0	0	26	1	1	50	6
d_{z^2}	$a_g\langle 73\rangle$	−0.6970	1	0	24	0	2	47	10
π_v–d_{yz}	$a_u\langle 21\rangle$	−0.8329	49	0	1	0	0	27	0
π_v–d_{yz}	$a_u\langle 20\rangle$	−0.9037	25	0	3	1	0	43	0
π^*_h–Fe(σ)	$a_g\langle 70\rangle$	−0.9076	36	16	16	4	0	11	3
π_h	$b_u\langle 46\rangle$	−1.1447	58	12	12	4	0	1	1
π_σ	$a_g\langle 65\rangle$	−1.2290	71	17	5	3	1	0	0
σ^*	$b_u\langle 42\rangle$	−1.5062	65	22	4	2	0	1	0

b. $[\{Fe(PH_3)(SH)_2(SH_2)_2\}_2(N_2H_2)]$ ($\tilde{\mathrm{II}}$)

orbital	label	energy (Rydberg)	charge decomposition[b] % N2	% H2	% Fe1	% S1	% S4	% S2	% S3	% P1
	$a_g\langle 78\rangle$	−0.2483	6	1	54	3	4	12	3	3
	$a_u\langle 49\rangle$	−0.2523	0	0	46	12	10	2	7	5
	$a_g\langle 77\rangle$	−0.2559	1	0	46	9	7	1	8	8
	$a_u\langle 47\rangle$	−0.2750	4	0	59	1	2	13	4	5
π^*_v–d_{yz}	$a_g\langle 74\rangle$	−0.3271	57	0	26	0	0	0	2	1
d_{xy}	$a_g\langle 76\rangle$	−0.4173	1	0	55	2	30	0	0	0
d_{xz}	$a_u\langle 46\rangle$	−0.4225	0	0	49	34	1	0	1	1
d_{xz}	$a_g\langle 75\rangle$	−0.4228	0	0	48	34	1	0	1	1
d_{xy}	$a_u\langle 48\rangle$	−0.4336	1	0	54	1	30	0	0	0
d_{xz}–π_v	$a_u\langle 45\rangle$	−0.4524	3	0	86	0	0	1	1	1
	$a_u\langle 44\rangle$	−0.4983	2	0	28	11	40	1	0	0
	$a_g\langle 73\rangle$	−0.5047	8	0	46	17	6	1	3	4
	$a_u\langle 43\rangle$	−0.5104	0	0	38	33	4	0	3	3
	$a_g\langle 71\rangle$	−0.5120	9	0	37	19	15	0	1	1
	$a_g\langle 72\rangle$	−0.5154	1	0	27	35	17	1	1	0
	$a_u\langle 42\rangle$	−0.5195	0	0	16	28	33	1	1	0
	$a_g\langle 70\rangle$	−0.5240	2	0	37	1	40	1	0	0
	$a_u\langle 41\rangle$	−0.6058	0	0	25	21	19	1	13	5
	$a_g\langle 69\rangle$	−0.6081	0	0	28	22	23	2	7	2
SH_2/PH_3	$a_u\langle 40\rangle$	−0.6195	1	0	16	7	9	1	23	21
SH_2/PH_3	$a_g\langle 67\rangle$	−0.6271	2	0	12	4	5	2	30	19
SH_2/d_{z^2}	$a_g\langle 66\rangle$	−0.6760	4	1	18	1	1	52	3	5
SH_2/d_{z^2}	$a_u\langle 38\rangle$	−0.6858	1	0	25	1	0	44	8	7
d_{z^2}	$a_g\langle 68\rangle$	−0.7250	3	0	23	2	4	9	24	17
d_{z^2}	$a_u\langle 39\rangle$	−0.7304	1	0	19	2	3	19	22	14
π_v–d_{yz}	$a_u\langle 35\rangle$	−0.8210	20	0	2	6	2	2	11	22
π_v–d_{yz}	$a_u\langle 33\rangle$	−0.8618	25	0	4	3	9	5	11	13
π_v–d_{yz}	$a_u\langle 32\rangle$	−0.8849	27	0	3	0	0	14	29	0
π^*_h–Fe(σ)	$a_g\langle 60\rangle$	−0.8895	45	11	16	0	1	13	1	2
π_h	$a_u\langle 29\rangle$	−1.1461	64	7	13	0	2	1	0	0
π_σ	$a_g\langle 56\rangle$	−1.3076	15	6	1	0	0	0	0	51
π_σ	$a_g\langle 54\rangle$	−1.3152	49	17	2	3	7	0	0	12
σ^*	$a_u\langle 24\rangle$	−1.6077	13	6	1	0	1	12	46	0
σ^*	$a_u\langle 23\rangle$	−1.6089	51	25	1	0	0	5	12	0

[a] From below −0.7 Rydberg only selected orbitals are listed. [b] If several symmetry-equivalent atoms exist, the charge decomposition gives the sum of all contributions.

participation of sulfur-p functions. Accordingly, e_g labels the σ-bonding combinations of d_{z^2} and $d_{x^2-y^2}$, which have S contributions of about 50% and 20−30% participation of Fe(II)-d orbitals (see Table 3a). The only important σ-bond not deriving from a sulfur-type orbital comes from the diazene π_h^* orbital; all other diazene σ-orbitals are too low in energy to interact with Fe(II)-d functions. In addition, two SH_2 lone pairs are found in the e_g-block.

(ii) Orbitals of Type t_{2g}^* and t_{2g}. The d_{xz} orbitals of both Fe(II) centers and the p-functions of the thiolate donors S_1 and S_3 form two linear combinations of symmetry b_g and a_u which both have about 50% Fe(II)-d and 35% S-p charge contribution. These two orbitals are practically degenerate and comprise the HOMO of the complex. The a_u-combination of the d_{yz} functions mixes only slightly with the diazene π_v orbital and remains nonbonding ($d_{yz}-\pi_v$), while the b_g-combination of d_{yz} strongly interacts with π_v^*. From this interaction, the LUMO of the complex results (see above). The d_{xy} orbitals of the Fe(II) centers, finally, lie within the Fe−N_2H_2−Fe-plane and have almost pure metal character, similar to $d_{yz}-\pi_v$.

The t_{2g}-block comprises the corresponding π-bonding orbitals. The bonding combination of d_{yz} (b_g-type) with π_v^*, called $d_{yz}-\pi_v^*$, interacts with the p-functions of the thiolate donors S_1 and S_3 and therefore splits (see above and Figure 3). Two of the remaining three orbitals in the t_{2g}-block are mostly thiolate lone pairs with 10% Fe-d contribution, and one consists of 40% d_{xz}- and 40% thiolate-p contribution. This is the bonding counterpart to the HOMO and shows the strong out-of-plane π-interaction between the thiolate donors and the Fe-d_{xz} orbitals. Two thiolate orbitals are found between the t_{2g}^*- and t_{2g}-block, which correspond to nonbonding combinations of the thiolate lone pairs. The almost pure metal character of the d_{xy} orbitals, on the other hand, demonstrates the weak π-interaction between the iron centers and the in-plane thiolate p-functions that are directed to the thiolate hydrogens. This is due to the fact that these orbitals are mostly hydrogen bonding. In model compound $\tilde{\mathrm{II}}$ the position of the thiolate hydrogens is altered in a way that the p lone pairs of two thiolates lie in the diazene-plane (see Figure 2), and consequently the interaction of these donors with the d_{xy} orbitals of iron is much stronger (see below).

Comparison with Complex $\tilde{\mathrm{II}}$. Using model complex $\tilde{\mathrm{II}}$ the MO-scheme for the phosphine containing compound II has been determined which is very similar to that obtained for I (see Figure 3). In particular, diazene is bound in the same way as in complex I. Differences result from the substitution of one of the thioether donors per iron center by phosphine and exchange of the amine donor in I by a thioether donor in II. Different also are the orientations of the thiolate lone pair orbitals. As a general result of the lower symmetry of $\tilde{\mathrm{II}}$, the basis functions of Fe(II) and sulfur mix stronger than in $\tilde{\mathrm{I}}$ leading to a larger covalency in $\tilde{\mathrm{II}}$. In particular, the p lone pairs of S_1 lying perpendicular to the diazene-plane interact with d_{xz} as in $\tilde{\mathrm{I}}$, whereas the p lone pairs of S_4 lie within the plane and strongly mix with the d_{xy} orbitals, which are no longer nonbonding as in $\tilde{\mathrm{I}}$. The comparison between S_1 and S_4 shows again that the covalent sulfur−hydrogen bonding p orbitals of the thiolates do not interact with iron orbitals, in contrast to the thiolate lone pairs. As a result of these interactions, there are now four orbitals in the energetic region of the HOMO which belong pairwise to the symmetric and antisymmetric combinations of d_{xz} and d_{xy}. In contrast, the a_u-combination of d_{yz}, called $d_{yz}-\pi_v$, has nearly pure iron-d character. The antibonding and bonding combinations of the orbital d_{yz} (a_g-type) with π_v^*, called $\pi_v^*-d_{yz}$ (LUMO) and $d_{yz}-\pi_v^*$, are very similar to model system $\tilde{\mathrm{I}}$ (see above).

Scheme 1

$$\begin{pmatrix} x \\ y \\ z \end{pmatrix} \longrightarrow a_u + 2b_u \qquad (\text{in } C_{2h})$$

a) MLCT
$\langle a_u \times a_u \times b_g \rangle = b_g$
$\boxed{\langle a_u \times b_u \times b_g \rangle = a_g}$

b) HOMO/LUMO
$\langle b_g \times \Gamma_u \times b_g \rangle = \Gamma_u$
$\langle a_u \times a_u \times b_g \rangle = b_g$
$\boxed{\langle a_u \times b_u \times b_g \rangle = a_g}$

Table 4. Comparison of the Calculated and Observed MLCT Energies (in cm^{-1})

method	"N_HS_4" (I)	"S_4P" (II)
Slater transition-state	14 160	16 620
experimental	17 240	16 130

The e_g^*-block consists of four orbitals which are closer in energy to each other than the corresponding orbitals in $\tilde{\mathrm{I}}$. The reason for this is the modification of the ligand field along the *z*-axis by substitution of one thioether donor by phosphine and in the *xy*-plane by substituting one amine ligand by one thioether per iron center. This is also reflected in the altered composition of the e_g^* orbitals as compared to $\tilde{\mathrm{I}}$. In the e_g-block, the d_{z^2} functions are smeared out over six orbitals with varying participations of p-functions of S_3 and the phosphine ligand. This indicates that phosphine and thioether have comparable ligand properties: they both are strong σ-donors with a very similar energy of the donating p-orbital. In contrast, the admixture of $d_{x^2-y^2}$ is restricted to the two e_g-orbitals of highest energy (see Table 3b).

C. UV−vis Spectroscopy. The UV−vis spectra of the diazene complexes I and II (Figure 6) show characteristic absorptions at 580 nm (I) and 620 nm (II), which in terms of the MO-scheme (Figure 3) can be assigned to the transition $d_{yz}-\pi_v \rightarrow \pi_v^*-d_{yz}$. Since $d_{yz}-\pi_v$ has about 90% iron-d character and $\pi_v^*-d_{yz}$ more than 50% diazene contribution (see Table 3a/b), these absorption bands correspond to a metal-to-ligand CT transition ("MLCT"), which is symmetry-allowed (Scheme 1). It is possible to perform two spin-unrestricted Slater transition state calculations[22] for the triplet (T) and mixed (U) state and then to compute the singlet excitation energy using the methodology of Ziegler et al.[23] Table 4 compares the experimental with the theoretical singlet MLCT energies obtained this way showing satisfactory agreement. The electronic transition from the a_u-symmetric HOMO to the LUMO is electric-dipole allowed (Scheme 1) and of MLCT type, too. Because of the vanishing overlap of HOMO and LUMO, this transition should nevertheless be of much smaller intensity than $d_{yz}-\pi_v \rightarrow \pi_v^*-d_{yz}$. The asymmetry of the observed absorption bands (see Figure 6) may therefore be due to the superposition of these two electronic transitions. Because of overlap considerations, the assignment of the high-intensity absorptions at 580 nm (I) and 620 nm (II) to the transition $d_{yz}-\pi_v \rightarrow \pi_v^*-d_{yz}$ is in any case plausible.

Further evidence that the observed absorptions belong to a charge-transfer transition between the Fe(II) centers and the diazene ligand comes from the resonance Raman spectroscopy. Different vibrations, especially the N−N-stretching mode, are significantly resonance enhanced in the Raman experiment, if the wavelength of the laser light used for scattering is in the region of MLCT absorption (cf. part 2 of this paper).

(22) Slater, J. C. *The Self-consistent Field for Molecules and Solids: Quantum Theory of Molecules and Solids*; McGraw-Hill: 1974; Vol. 4.

(23) (a) Ziegler, T.; Rauk, A.; Baerends, E. J. *Theor. Chim. Acta* **1977**, *43*, 261. (b) Ziegler, T. *Chem. Rev.* **1991**, *91*, 651.

Discussion

A. Electronic Structure of Complexes I and II. The electronic structure of the Fe−diazene systems has been determined with the help of Mössbauer and UV−vis spectroscopy coupled to SCF-Xα-SW calculations. The Mössbauer data unambigously indicate a Fe(II) low-spin configuration for the iron centers. This assignment is in accordance with Mössbauer and structural data on analogous [Fe(L)'N_HS_4'] systems with various coligands L.[19] While the diazene systems show a close similarity to the L = CO complex, systems with purely σ-donating ligands, L, like N_2H_4, amines, and CH_3OH, exhibit significantly longer Fe-S and Fe−N(amine) bonds and show Mössbauer parameters indicative of a Fe(II) high-spin configuration. Therefore, the 'N_HS_4' ligand (and in analogy the 'S_4'-phosphine ligand system) generates an intermediate ligand field such that the bonding properties of the coligand L determine the spin-state of the Fe centers.

Using the information from the Mössbauer data obtained on complex I and II, SCF-Xα -SW calculations of the electronic ground state as well as Slater transition-state calculations have been carried out on structural models $\tilde{\mathrm{I}}$ and $\tilde{\mathrm{II}}$ for complexes I and II, respectively. These calculations have led to a clear picture of the bonding of diazene to Fe−sulfur centers with octahedral ligand sphere: The HOMO of diazene (π_h^*), which is N−N antibonding and N−H bonding is strongly lowered in energy by a σ-interaction with the d-orbitals (of type e_g) of iron. Due to this strong σ-bond from its HOMO, diazene primarily acts as a σ-donor.[24] This is the main contribution to the iron−diazene bond. The lowest unoccupied MO of diazene (π_v^*) is situated slightly above the fully occupied t_{2g}^* manifold of the iron centers and is raised in energy due to a π-interaction with the metal-d_{yz} orbitals. This leads to a LUMO of the complex that is of >50% diazene character whose energy lies between the occupied t_{2g}^* and empty e_g^* metal orbitals. The corresponding bonding combination between d_{yz} and π_v^* is strongly lowered in energy by a large π-interaction. Hence, diazene also acts as a good π-acceptor due to its low-lying LUMO. In contrast, the orbital π_v is at very low energy and only shows a small interaction with Fe(II)-d functions. Therefore, diazene is by no means a π-donor ligand. The HOMO of both complexes I and II consists of an almost degenerate pair of d_{xz} orbitals (symmetric and antisymmetric combination) which are nonbonding with respect to the diazene unit but strongly mixed with out-of-plane thiolate lone pairs. Therefore, oxidation of the compounds should lead to the formation of Fe(III) and not affect the bound diazene. The HOMO−LUMO gap is roughly 1 eV. If in-plane thiolate lone pairs also are present, the d_{xy} orbitals are raised in energy as well and become located in the region of the HOMO. This demonstrates the strong π-donor function of the thiolate lone pairs. In contrast, the π -donor character of the sp hybridized S−C orbitals (S−H orbitals in our models) of the thiolate and thioether groups is weak.

A final contribution to the stabilization of the Fe−diazene bond in the complexes I and II derives from the hydrogen bonds between the thiolate donors and the diazene protons. This interaction is manifested in a delocalization of various diazene-type orbitals with N−H bonding character toward the thiolate atoms with the shorter S−H(diazene) distance (2.36 Å in II[14]) being contained in the S−Fe−N−N−H five-membered ring. In the "S_4"-phosphine system (complex II), these are the thiolate atoms having in-plane lone pairs (out-of-plane S−C(phenyl) bonds, see Figure 2). In contrast, no such delocalization is observed toward the thiolate donors with the longer S−H bond (2.81 Å in II[14]) contained within the Fe−S−N−H four-membered ring (see Figure 5). In the "S_4"-phosphine system, these thiolates have out-of-plane lone pairs (in-plane S−C(phenyl) bonds). It is likely that the preference for the formation of a hydrogen bond with the thiolate ligand having an in-plane lone pair is the driving force behind the selective crystallization of one diastereomer (= complex II) in the 'S_4'-phosphine system. In the corresponding diastereomer, the S−H bond within the five-membered ring is directed toward a thiolate ligand having an out-of-plane lone pair (cf. part 2 of this paper). In that case the hydrogen bond is mediated by the sp-hybridized orbital of the S−C bond within the diazene-plane, but the interaction is weaker. This is demonstrated in the [{Ru'S_4'-(PPh_3)}$_2$(N_2H_2)] complex[25] exhibiting this conformation, where the S−H bond within the five-membered ring actually becomes longer than in the four-membered ring.

Based on the ground state electronic-structure description and SCF-Xα transition-state calculations, the 620 and 580 nm bands of complex II and I, respectively, are assigned to metal-to-ligand charge-transfer transitions (MLCTs) from the iron(II) d_{yz} orbitals into the diazene-type LUMO. These bands have previously been assigned to the lowest-energy transition of a diazene-iron four-center-6π-electron system.[26] In fact this scheme is qualitatively reproduced in our calculation; the relevant out-of-plane π-orbitals are shown in Figure 5. Note the increase of the number of nodes from 0 in π_v–d_{yz} to 3 in π_v^*–d_{yz}. However, this formulation exaggerates the covalency of the Fe−diazene system since the two orbitals at highest energy are in fact primarily of metal (d_{yz}–π_v) and diazene (π_v^*–d_{yz}) character, respectively. Hence, a MLCT interpretation of the 580 and 620 nm band, respectively, appears more appropriate. This assignment is also supported by the resonance enhancement behavior of the diazene vibrations (cf. part 2 of this paper). The HOMO−LUMO transition corresponds to a MLCT transition as well and is electric-dipole allowed. However, its intensity is very weak since the d_{xz} orbitals are oriented perpendicular to the Fe−diazene bond.

B. Chemical Reactivity and Relevance to the Nitrogenase Problem. Following the procedure of Sellmann et al.[13,14] compounds I and II can be synthesized by oxidation of the corresponding, in situ formed, hydrazine complexes by air. The question arises as to whether Fe−sulfur centers also can be used in the reverse direction to generate hydrazine or even ammonia from diazene. This is of relevance with respect to the question of whether or not diazene is involved in the reduction of dinitrogen by nitrogenase. While no unambiguous evidence exists for diazene as an intermediate in the reduction of dinitrogen by nitrogenase,[27] the enzyme does reduce the diazene derivatives diazirine and *trans*-dimethyldiazene.[28] On the other hand, Thorneley and Lowe suggest that isodiazene ($N-NH_2$) and not diazene (HN−NH) is the relevant intermediate of enzymatic dinitrogen reduction at the diazene level.[8] Corresponding Mo=N−NH_2 "diazenido (2−)" complexes have been shown to be involved in the generation of NH_3 from N_2 bound end-on to Mo(0) centers.[7] How can one envisage a parallel iron-centered reduction of diazene to hydrazine or ammonia? In the present diazene model systems, the iron centers are octahedrally coordinated by sulfur coligands and have a Fe(II) low-spin d^6 configuration; i.e., the t_{2g}^* manifold is fully occupied and the e_g^* orbitals are empty (see Scheme 2). The

(24) Albini, A.; Kisch, H. *Top. Curr. Chem.* **1976**, *65*, 105.

(25) Sellmann, D.; Böhlen, E.; Waeber, M.; Huttner, G.; Zsolnai, L. *Angew. Chem.* **1985**, *97*, 984.

(26) Sellmann, D. *Angew. Chem.* **1974**, *86*, 692.

(27) *Molybdenum Enzymes*; Spiro, T. G., Ed.; John Wiley: 1985.

(28) McKenna, C. E.; Simeonov, A. M.; Eran, H.; Bravo-Leerabhandh, M. *Biochemistry* **1996**, *35*, 4502.

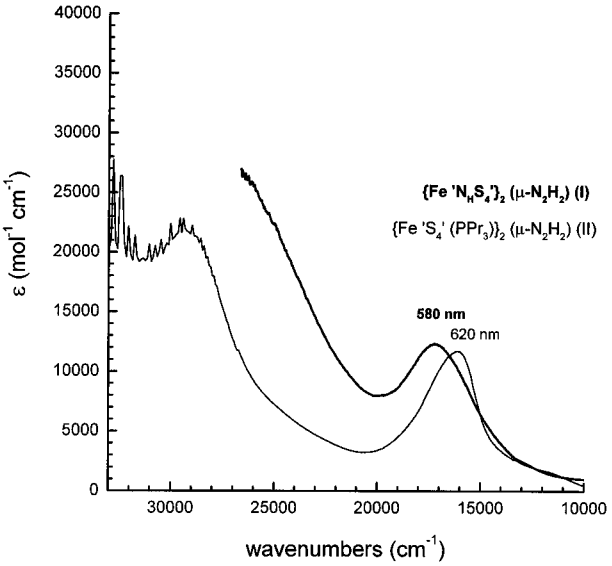

Figure 6. UV−vis spectra of complexes I and II in THF at room temperature.

Scheme 2

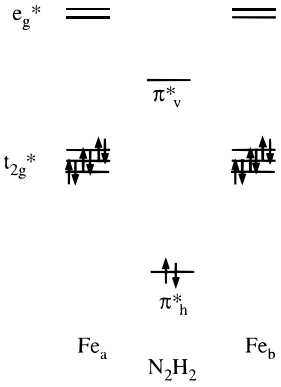

Scheme 3

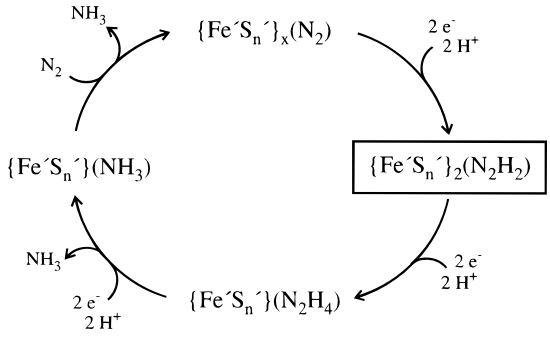

diazene unit is only moderately activated toward protonation and therefore needs to be reduced first. Importantly, our calculations and the spectroscopic data show that the diazene π^*_v orbital is the LUMO of the complex. *Therefore, transfer of electrons to the diazene complex directly leads to the reduction of the N_2H_2* ligand (Scheme 3; "S_n" = 'N_HS_4' and 'S_4'(PPr_3)). This is in contrast to the [Fe(CO)'N_HS_4'] complex where transfer of electrons causes reduction to Fe(I) and Fe(0) complexes due to the higher energy of the CO π^* orbitals.[29] Protonation of the $N_2H_2^{2-}$ species then completes the change from a N−N double to a N−N single bond and leads to a loss of backbonding. This in turn causes the iron centers to become high-spin (note that all [Fe(L)'N_HS_4'] systems with purely σ-donating ligands

(29) Sellmann, D.; Becker, T.; Knoch, F. *Chem. Eur. J.* **1996**, *2*, 1092.

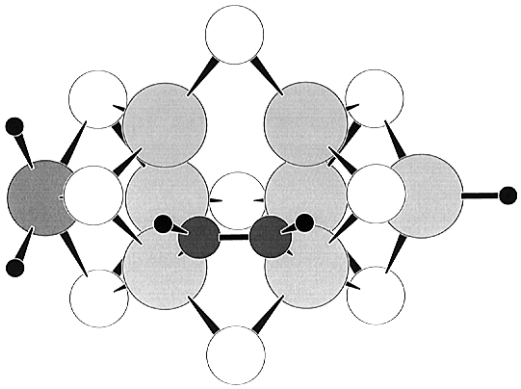

Figure 7. Possible coordination of diazene to the FeMoCo of the enzyme nitrogenase. The FeMoCo model is adapted from ref 5a. Bond distances of diazene are taken from ref 13.

are high-spin). The high-spin Fe(II) species is kinetically labile such that, at this stage, one Fe−N bond probably breaks apart, and a Fe−N_2H_3 species results which is protonated to the Fe−N_2H_4 complex (Scheme 3). Further reduction of N_2H_4 to NH_3 depends on the lability of the Fe−N bond. In case the ligand is lost at this stage (i.e., the second Fe−N bond breaks), reduction ends at the hydrazine level. If, on the other hand, the remaining Fe−N bond is sufficiently strong to keep the ligand, protonation of the hydrazine ligand at the lone pair of the β-nitrogen leads to N−N cleavage, liberation of NH_3, and formation of an Fe−imino species which can be further reduced and protonated to give one more molecule of ammonia. Bonding of N_2 (Scheme 3, top; $x = 1, 2$) completes this catalytic cycle which has been proposed before.[19]

If the ligand system "S_n" in the reduction pathway of Scheme 3 is 'N_HS_4' or 'S_4'(PPr_3), the diazene complexes (framed) cannot be reduced at accessible potentials since their LUMOs are too high in energy. Note that an estimate of the reduction potential is possible, based on the value of the HOMO/LUMO gap, which approximately should correspond to the difference between the potentials of Fe oxidation (Fe(II) → Fe(III) = first oxidation potential = −0.11 eV for the "S_4P" complex) and diazene reduction. With a calculated HOMO−LUMO gap of approximately 1 eV (see Table 3a/b), the first reduction potential for complexes I and II should be at about −1 V. At this negative potential, however, the diazene protons are reduced to H_2 which in practice leads to destruction of the complex. Nevertheless, the proposed reduction pathway is of relevance to the nitrogenase problem considering that the iron centers of the FeMoCo are contained within a cubane-like structure with a highly unusual, approximately trigonal-planar, coordination by sulfur ligands. End-on bonding of diazene to one or two iron centers of the FeMoCo could lead to a nearly planar S_3N-ligation which exhibits a ligand field strength that is much weaker than in the octahedrally coordinated model compounds (Figure 7). Therefore, the iron centers are in a high-spin Fe(II)/Fe(III) state, and metal orbitals become occupied that are at higher energy than the π^*_v orbital of diazene (Scheme 4, left). Correspondingly, the Fe(II)−N_2H_2−Fe(II) configuration is unstable and immediately changes to a Fe(III)−$N_2H_2^{2-}$-Fe(III)-structure (Scheme 4, right) in which the diazene ligand is reduced and the two Fe(III) high-spin centers are antiferromagnetically coupled: *the iron high-spin configuration allows the flow of electrons to the diazene-ligand at physiological reduction potentials due to the fact that the diazene π^*_v orbital is at lower energy than occupied metal-3d orbitals.* Whereas the Fe(II) low-spin configuration in the binuclear model systems is necessary to stabilize the diazene ligand and the complex geometry, the substrate being reduced at the FeMoCo has many bonding sites

Scheme 4

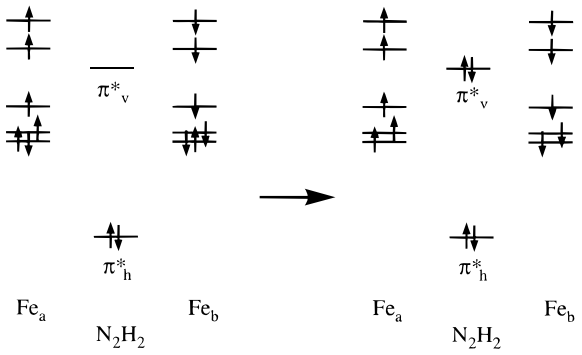

on a multiply connected metal framework and therefore is not lost even if it is bound to high-spin metal centers. Of course, the protein environment may also contribute to keep the partly reduced substrate bound to the cofactor.

Whereas the isodiazene intermediate proposed by Lowe and Thorneley (see above) should be involved in a reduction pathway starting from end-on (asymmetrically) bound N_2, the presence of diazene as an intermediate is easier to reconcile with an initial edge-on (symmetric) bonding of dinitrogen involving both N atoms.[2a] Edge-on or side-on bound dinitrogen is known to be highly activated[4] and therefore can be protonated to give diazene. Further reduction and protonation of this species could occur as described in Scheme 3 leading to a N_2H_4-intermediate; rearrangement to terminal end-on bonding and further protonation/reduction finally would generate two molecules of NH_3. Based on the electronic structure description of the Fe/S-diazene systems obtained in this study, this "side-on" or "symmetric" reduction pathway involving diazene as an intermediate remains a realistic alternative for the mechanism of nitrogenase to the previously proposed "asymmetric" pathway starting from end-on terminally bound dinitrogen.

Acknowledgment. F.T. gratefully acknowledges the support of these investigations by the Deutsche Forschungsgemeinschaft (Grant Tu58/4-1 and Tu58/5-1) and thanks P. Bellm for recording the Mössbauer spectra of compound I. N.L. thanks the Fonds der Chemischen Industrie for a Kekulé Research Fellowship.

JA970419Y